RSC Advances

PAPER

View Article Online
View Journal | View Issue

Cite this: *RSC Adv.*, 2017, **7**, 47933

A high-temperature organic–inorganic ferroelectric with outstanding switchable dielectric characteristics†

Cong Xu, Wenjun Zhang, Linsong Gao, Xuecheng Gan, Xiaofan Sun, Zepeng Cui, Hong-Ling Cai* and X. S. Wu*

Received 14th September 2017
Accepted 5th October 2017

DOI: 10.1039/c7ra10221f

rsc.li/rsc-advances

A new molecular ferroelectric is discovered in an organic–inorganic hybrid compound, $(C_6H_5NH_3)_2CdCl_4$, which undergoes a reversible order–disorder ferroelectric phase transition at 369 K and has a spontaneous polarization of about 0.5 μC cm^{-2}, larger than the Rochelle salt. Large dielectric anomaly, pyroelectricity and P–E hysteresis loop were observed to represent the ferroelectricity of the compound. Especially, the dielectric constant at the transition temperature increases more than 40 times than that at room temperature, which indicates potential applications on switches and sensors for its high-temperature response and excellently reversible characterization.

Introduction

Ferroelectrics are multifunctional phase transition materials, which have multiple physical properties, such as pyroelectricity, piezoelectricity, dielectricity, second harmonic generation (SHG) and electro-optic effects. These have aroused much interest for their potential applications in switches, sensors, memory devices and nonlinear optical (NLO) devices.[1–4] As one class of ferroelectrics, molecular ferroelectrics, have more advantages of light weight, good processability, mechanical flexibility and structural tenability.[5–8] A series of compounds composed by ammonium cations and acid ions have been found, namely, diisopropylammonium bromide (DIPAB),[1,9,10] diisopropylammonium perchlorate,[11,12] 4-(cyanomethyl)anilinium perchlorate,[13] 4-methoxy anilinium tetrafluoroborate 18-crown-6,[14] (4-amino-2-bromopy ridinium)(4-amino-2-bromopyridine) tetrafluoroborate,[15] pyridin-4-yl-methanaminium perchlorate,[16] which have outstanding phase transition and ferroelectric characteristics. Therefore, a huge potential in practical applications can be foreseen in the coming future.

In recent years, the organic–inorganic hybrid ferroelectrics have caused much attention for the designable and tuneable characteristics of organic and inorganic components. So far, quite a few so called one- or three-dimensional organic–inorganic ferroelectrics have been discovered, such as (pyrrolidinium)MnX_3 (X = Cl, Br),[17,18] (pyrrolidinium)$CdCl_3$,[19] (cyclopentylammonium) $CdCl_3$,[20] (3-pyrrolinium)MCl_3 (M = Mn, Cd),[21,22] metal–organic framework,[23,24] and so forth. In addition, the substitution method is often used to discover new ferroelectrics, for example, [MeH-dabco]RbI_3 performs ferroelectric property while [H_2dabco]RbI_3 does not.[25] Moreover, lead-halide layered perovskite-type ferroelectrics have drawn great public concern for their illustrious photovoltaic properties. The structure of layered perovskite-type ferroelectrics (A_2BX_4, A is a monovalent organic ammonium, B is a divalent transition metal, and X is a halogen) can be described as orderly arranged layers of corner-sharing (BX_6) octahedra sandwiched by the bilayers of organic ammonium cations. Some pre-existing compositions, such as (benzylammonium)$_2PbCl_4$,[26] (cyclohexylammonium)$_2PbBr_{4-4x}I_x$ (x = 0–1),[27] not only have shown excellent ferroelectricity but also make steps toward molecular-based semiconductors.

Experimental

The compound of $(CHA)_2CdCl_4$ (CHA = cyclohexylammonium) is a layered perovskite-type ferroelectric with high phase transition temperature. It was synthesized by the solution growth method. 10 mmol cyclohexylammonium (CHA) chloride and 5 mmol cadmium chloride were dissolved in 20 mL deionized water. A colorless clear solution was obtained after continuous stirring. Then colorless block crystals were obtained by slowly evaporating at room temperature after a few weeks. All reagents and solvents in the syntheses were of reagent grade and used without further purification. Polycrystalline samples for Powder X-Ray Diffraction (PXRD) were prepared by grinding the air-dried crystals into fine powder.

Several measurements to represent the characteristics of phase transition, dielectricity and ferroelectricity were made. Differential scanning calorimetry (DSC) and heat capacity measurements of the single crystals were performed on NETZSCH DSC 200 F3 under nitrogen protection in aluminum crucibles with a heating

Collaborative Innovation Center of Advanced Microstructures, Lab of Solid State Microstructures, School of Physics, Nanjing University, Nanjing 210093, P. R. China. E-mail: hlcai@nju.edu.cn; xswu@nju.edu.cn

† Electronic supplementary information (ESI) available. See DOI: 10.1039/c7ra10221f

or cooling rate of 10 K min^{-1}. Variable-temperature single-crystal X-ray diffraction analysis was carried out using a Rigaku Saturn 724+ CCD diffractometer equipped with Mo Kα radiation (λ = 0.71073 Å). Data collection, cell refinement, and data reduction were performed using Rigaku Crystalclear 1.3.5. The structures of crystals were solved by direct methods and refined by the full matrix method based on F2 using the SHELXLTL software package. All non-hydrogen atoms were refined anisotropically, and the positions of all hydrogen atoms were generated geometrically. For dielectric, pyroelectric, P–E hysteresis loops measurement, the single crystals were cut into thin plate. Silver conductive paste deposited on the plate surfaces was used as the electrodes. The complex permittivity measurement was using Tonghui TH2828A LCR meter at the frequency from 20 Hz to 1 MHz with an applied electric field of 0.5 V. The pyroelectric current was measured using Keithley 6517B electrometer. The P–E hysteresis loops were recorded on a Precision Premier II (Radiant Technologies, Inc.).

Results and discussion

The DSC measurement is a useful and intuitionistic way to detect whether a crystal displays a reversible phase transition triggered by heating and cooling. We performed DSC measurement in the temperature range 303–393 K (Fig. 1). The DSC curve shows an endothermic peak at 369 K (T_c) and an exothermic peak at 344 K (T'_c). Here the structural phases above and below T_c are labelled as the high-temperature phase (HTP) and the room-temperature phase (RTP). The noteworthy thermal hysteresis of about 25 K indicates a first-order phase transition. The entropy changes of phase transitions can be calculated as $\Delta S = \Delta H/T$, where the value of enthalpy change ΔH can be integral from the peak area of DSC anomalies. The enthalpy change is $\Delta H = 22.41$ J g^{-1} for the phase transition at 369 K in heating progress, corresponding to the entropy change of $\Delta S = 112.28$ J (mol^{-1} K^{-1}). From the Boltzmann equation ($\Delta S = R \ln N$, where R is gas constant and N represents ratio of possible configurations),[27] it is found that $N = 2.60$, indicating that the phase transition at 369 K is ascribed to an order–disorder type.

The ferroelectricity is often supported by the large dielectric anomalies. The dielectric behavior of the compound was measured at a low-frequency range from 500 to 1 MHz with the temperature changing from 320 to 480 K (Fig. 3). The dielectric constant at the frequency of 500 Hz along the c axis increases abruptly from 50 to 2100 at around T_c = 369 K in the heating process. The changing ratio is up to 42, which indicates that this compound is also a candidate of dielectric switching materials.

The compound crystallizes in a space group of $Cmc2_1$ at the temperature of 293 K (RTP), which belongs to the C_{2v}, one of the ten polar point groups. The NH_3 groups of CHA cations orient in the cavities enclosed by $CdCl_6$ octahedrons, and the corner-sharing octahedra layers are between CHA bilayers (Fig. 2a). The CHA cations form N–H···Cl hydrogen bonds with the $[CdCl_4]_n^-$ chains, resulting in stabilizing the hybrid structure. From the viewpoint of polarization, the characteristic feature of the structure is that all the C–N bonds of CHA cations align along the c-axis (Fig. 2c). The structure in the HTP was refined with the non-polar space group $I222$, in which the configuration of the $[CdCl_4]_n^-$ shows a marked difference. The Cd atoms form a linear chain along the c axis, because the Cd–Cd–Cd angle within the chain becomes 180° (Fig. 2b). Every Cl atom aligns orderly between two adjacent Cd atoms in the c direction. Nevertheless, The Cl atoms in the a axis and b axis are disordered over two sites related by a 2-fold rotation axis where

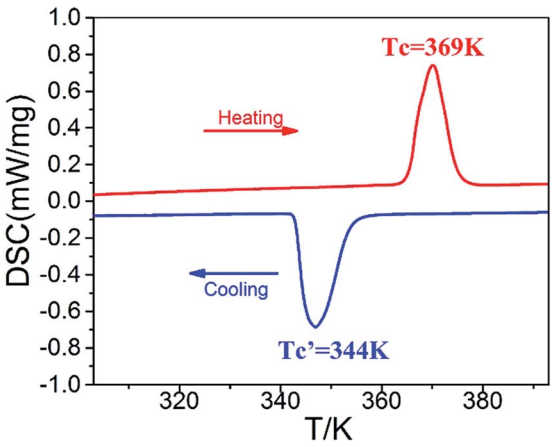

Fig. 1 Temperature dependence of DSC curve at a rate of 10 K min^{-1} for the compound.

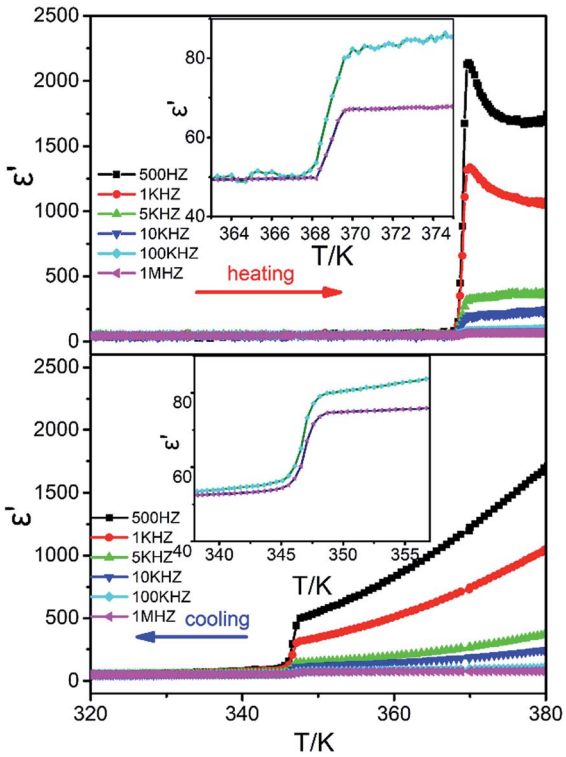

Fig. 2 Temperature-dependence of real part (ε') of complex dielectric constant of the compound in heating process and cooling process. Inset: the dielectric constant at the frequency of 100 KHz and 1 MHz in heating and cooling process.

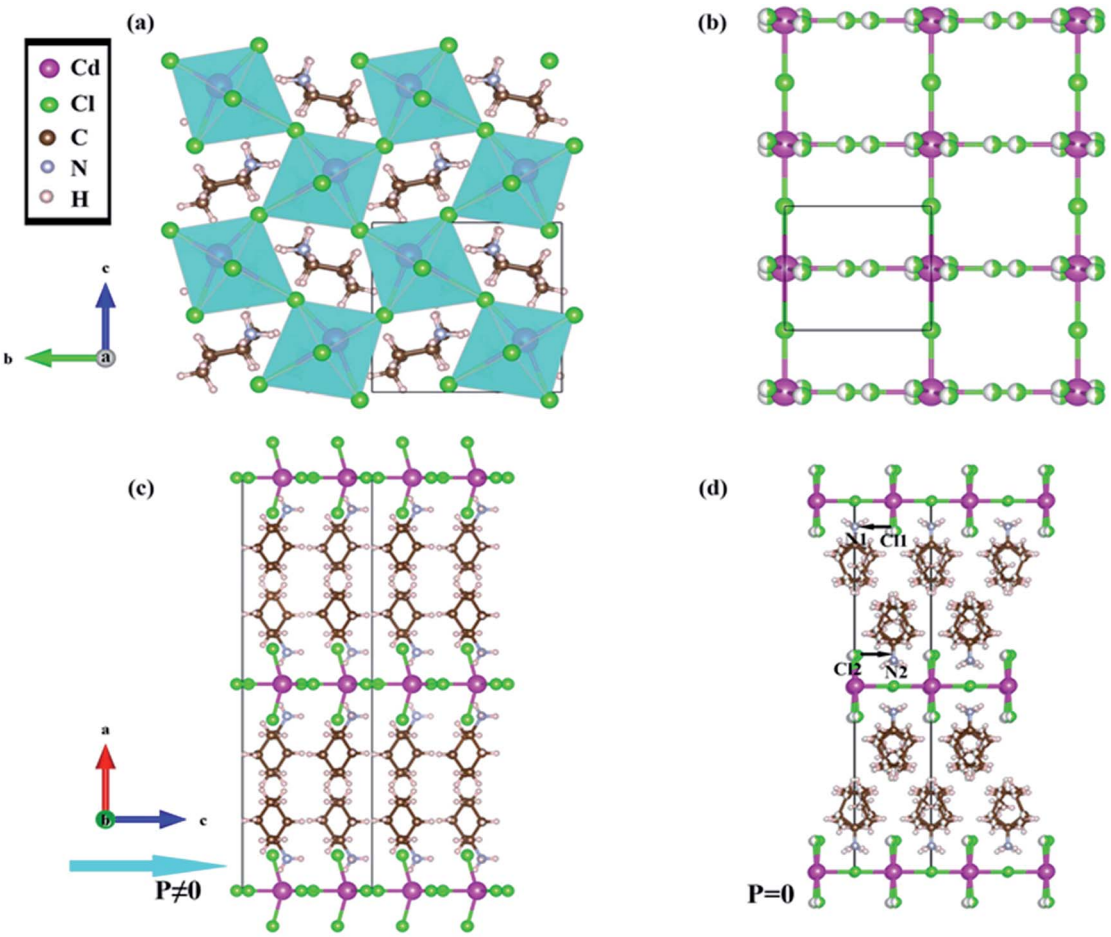

Fig. 3 Crystal structure diagrams of the compound: (a) along *a* axis at 293 K; (b) along *a* axis at 383 K; (c) along *b* axis at 293 K, the polarization is along *c* axis; (d) along *b* axis at 383 K.

located the Cd atoms. Thus the CHA cations are highly disordered over two positions related by a 2-fold rotation axis along the *a* axis. The direction of the dipole of Cl1–N1 is antiparallel with that of the dipole of Cl2–N2, so the compound shows paraelectric features in the HTP. Considering the change of the structure between the RTP and HTP, we suppose that the origin of ferroelectricity of the compound is the order–disorder of the ammonium cations.

Ferroelectrics are definitely pyroelectric materials, therefore the spontaneous polarization of ferroelectrics can be determined from pyroelectric behavior. The excess free charges appear on the polar surfaces of the ferroelectric crystal when temperature-dependent spontaneous polarization changes, which can give rise to the detectable pyroelectric current in the circuit between the two opposite polar surface. The pyroelectric current was measured under zero electric field in the heating and cooling processes. Since the crystal is free for expansion on heating, the secondary or constant-stress pyroelectric effect was measured, which is attributed to both piezo- and pyro-electric components. The spontaneous polarization can be integrated as: $P_s = \int \frac{i}{AR} dT$, where i is the current, A is the area of sample, and R is the heating/cooling rate. Before measurement, the sample was polarized with a voltage of 300 V for about 5 min at room temperature. A temperature-depended pyroelectric current was recorded (Fig. 4a), where a peak with value of 0.14 nA was observed at 369 K, indicating the release of screen charge. The integral polarizations under a polarizing voltage of 300 V are about 0.4 μC cm^{-2} in RTP and 0 in HTP. Similarly, the pyroelectric current peak reversed when the sample was polarized with a voltage of −300 V. This step-like pyroelectric anomaly indicates a ferroelectric–paraelectric phase transition (space group transition from $Cmc2_1$ to $I222$).

In addition, the pyroelectric current can be measured in another method, the Chynoweth technique, by recording the pyroelectric current due to the periodic changing of the temperature by turning on or off an infrared laser. When the laser is turned on, the temperature of the sample increases quickly and then reaches a constant value. The pyroelectric current sharply jumps to maximal value of about 0.08 nA and slowly approaches almost zero. Similarly, the process how the current changes when the pulse laser is turned off appears an opposite tendency (Fig. 4b). This method excludes effects like trapped charge or electrets from pyroelectric current measurement, so it clearly shows the pyroelectric characterization of the compound.

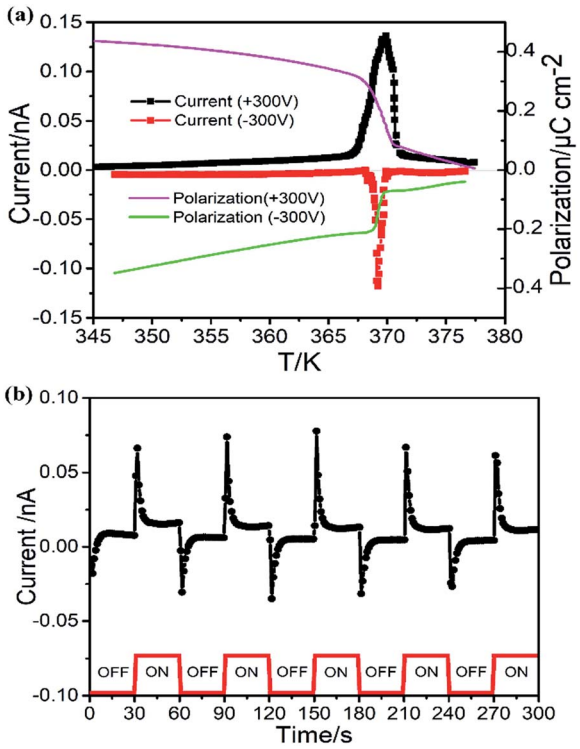

Fig. 4 (a) The temperature-dependent pyroelectric currents of the compound polarized by opposite electric voltages (±300 V) and the temperature dependence of polarization determined by integration of pyroelectric currents. (b) Pyroelectric current density of the compound modulated by a pulse laser at room temperature.

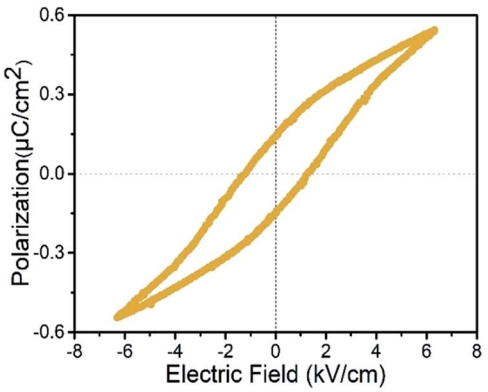

Fig. 5 P–E hysteresis loops at 313 K measured along *c*-axis with a frequency of 50 Hz.

The most direct way to verify the ferroelectric is the measurements of typical polarization–electric field (P–E) hysteresis loops, which can confirm the ferroelectric polarization reversal. At ferroelectric phase, the coercive field becomes smaller with the temperature increasing. The polarization will disappear at the temperature higher than ferroelectric–paraelectric phase transition point. It presented 'S'-shaped curves just below T_c at a frequency of 50 Hz (Fig. 5). The ferroelectric hysteresis loop measured at 313 K clearly shows that the spontaneous polarization (P_s) is 0.53 μC cm^{-2} and remnant polarization (P_r) is 0.14 μC cm^{-2}. The value of spontaneous polarization is a little larger than those of Rochelle salt (0.2 μC cm^{-2}), [(2,6-diisopropylanilinium)([18]crown-6)]BF_4 (0.3 μC cm^{-2}),[28] ammonium sulfate (0.25 μC cm^{-2}) and [4-$NH_2C_5H_4NH$][$SbCl_4$] (0.35 μC cm^{-2}),[29,30] but much smaller than those of diisopropylammonium bromide (*ca.* 23 μC cm^{-2}),[1] croconic acid (*ca.* 20 μC cm^{-2}),[31] (benzylammonium)$_2PbCl_4$ (13 μC cm^{-2})[26] and PVDF (8 μC cm^{-2}).

Conclusions

In summary, we present that the organic–inorganic hybrid compound $(CHA)_2CdCl_4$ is a molecular ferroelectric with a spontaneous polarization of 0.53 μC cm^{-2}, and reveal that its ferroelectric mechanism arises from the order–disorder transition of the CHA cations. The compound undergoes a ferroelectric–paraelectric phase transition at $T_c = 369$ K, which indicates its great potential on applications under a wide range of temperature. Particularly, the intriguing thing is the large changing ratio of temperature-dependent dielectric constant, which is up to 42 times. Moreover, the high-temperature response characterization and outstanding reversibility of dielectricity make it possible to be applied as switches and sensors under variable conditions.

Conflicts of interest

There are no conflicts to declare.

Acknowledgements

This work was supported by the National Natural Science Foundations of China (11574138, 21427801, U1332205, 11274153), the Top-Notch Young Talents Program of China, the National Key R&D Program of China (2016YFA0201104), the Project 973 (2014CB848800), and Dengfeng Project B of Nanjing University.

Notes and references

1 D. W. Fu, H. L. Cai, Y. M. Liu, Q. Ye, W. Zhang, Y. Zhang, X. Y. Chen, G. Giovannetti, M. Capone, J. Y. Li and R. G. Xiong, *Science*, 2013, **339**, 425–428.
2 L. Pan, G. Liu, H. Li, S. Meng, L. Han, J. Shang, B. Chen, A. E. Platero-Prats, W. Lu and X. Zou, *J. Am. Chem. Soc.*, 2014, **136**, 17477–17483.
3 O. Sato, *Nat. Chem.*, 2016, **8**, 644–656.
4 J. Scott, *Science*, 2007, **315**, 954–959.
5 S. Horiuchi and Y. Tokura, *Nat. Mater.*, 2008, **7**, 357–366.
6 F. Jona and G. Shirane, *Ferroelectric crystals*, Pergamon, 1962.
7 G. Smolenskiĭ, *Ferroelectrics and related materials*, Taylor & Francis, US, 1984.
8 W. Zhang and R.-G. Xiong, *Chem. Rev.*, 2011, **112**, 1163–1195.
9 K. Gao, C. Liu, Z. Cui, J. Zhu, H.-L. Cai and X. Wu, *CrystEngComm*, 2015, **17**, 2429–2432.
10 K. Gao, C. Xu, Z. Cui, C. Liu, L. Gao, C. Li, D. Wu, H.-L. Cai and X. Wu, *Phys. Chem. Chem. Phys.*, 2016, **18**, 7626–7631.

11 K. Gao, Z. Cui, C. Liu, J. Zhu, H.-L. Cai and X. Wu, *RSC Adv.*, 2015, **5**, 62647–62651.
12 K. Gao, M. Gu, X. Qiu, X. Ying, H.-Y. Ye, Y. Zhang, J. Sun, X. Meng, F. Zhang and D. Wu, *J. Mater. Chem. C*, 2014, **2**, 9957–9963.
13 H.-L. Cai, W. Zhang, J.-Z. Ge, Y. Zhang, K. Awaga, T. Nakamura and R.-G. Xiong, *Phys. Rev. Lett.*, 2011, **107**, 147601.
14 D.-W. Fu, H.-L. Cai, S.-H. Li, Q. Ye, L. Zhou, W. Zhang, Y. Zhang, F. Deng and R.-G. Xiong, *Phys. Rev. Lett.*, 2013, **110**, 257601.
15 C. Liu, K. Gao, Z. Cui, L. Gao, D.-W. Fu, H.-L. Cai and X. S. Wu, *J. Phys. Chem. Lett.*, 2016, **7**, 1756–1762.
16 Z. Cui, K. Gao, C. Liu, Y. Yin, D.-W. Fu, H.-L. Cai and X. S. Wu, *J. Phys. Chem. C*, 2016, **120**, 2925–2931.
17 Y. Zhang, W. Q. Liao, D. W. Fu, H. Y. Ye, C. M. Liu, Z. N. Chen and R. G. Xiong, *Adv. Mater.*, 2015, **27**, 3942–3946.
18 Y. Zhang, W.-Q. Liao, D.-W. Fu, H.-Y. Ye, Z.-N. Chen and R.-G. Xiong, *J. Am. Chem. Soc.*, 2015, **137**, 4928–4931.
19 W. J. Xu, C. T. He, C. M. Ji, S. L. Chen, R. K. Huang, R. B. Lin, W. Xue, J. H. Luo, W. X. Zhang and X. M. Chen, *Adv. Mater.*, 2016, **28**, 5886–5890.
20 Y. Zhang, H.-Y. Ye, W. Zhang and R.-G. Xiong, *Inorg. Chem. Front.*, 2014, **1**, 118–123.
21 H. Y. Ye, Y. Zhang, D. W. Fu and R. G. Xiong, *Angew. Chem., Int. Ed.*, 2014, **53**, 11242–11247.
22 H.-Y. Ye, Q. Zhou, X. Niu, W.-Q. Liao, D.-W. Fu, Y. Zhang, Y.-M. You, J. Wang, Z.-N. Chen and R.-G. Xiong, *J. Am. Chem. Soc.*, 2015, **137**, 13148–13154.
23 Y. Tian, S. Shen, J. Cong, L. Yan, S. Wang and Y. Sun, *J. Am. Chem. Soc.*, 2016, **138**, 782–785.
24 G.-C. Xu, X.-M. Ma, L. Zhang, Z.-M. Wang and S. Gao, *J. Am. Chem. Soc.*, 2010, **132**, 9588–9590.
25 W.-Y. Zhang, Y.-Y. Tang, P.-F. Li, P.-P. Shi, W.-Q. Liao, D.-W. Fu, H.-Y. Ye, Y. Zhang and R.-G. Xiong, *J. Am. Chem. Soc.*, 2017, **139**, 10897–10902.
26 W.-Q. Liao, Y. Zhang, C.-L. Hu, J.-G. Mao, H.-Y. Ye, P.-F. Li, S. D. Huang and R.-G. Xiong, *Nat. Commun.*, 2015, **6**, 7338.
27 H.-Y. Ye, W.-Q. Liao, C.-L. Hu, Y. Zhang, Y.-M. You, J.-G. Mao, P.-F. Li and R.-G. Xiong, *Adv. Mater.*, 2016, **28**, 2579–2586.
28 H.-Y. Ye, S.-H. Li, Y. Zhang, L. Zhou, F. Deng and R.-G. Xiong, *J. Am. Chem. Soc.*, 2014, **136**, 10033–10040.
29 R. Jakubas, Z. Ciunik and G. Bator, *Phys. Rev. B*, 2003, **67**, 024103.
30 G. Bator and R. Jakubas, *J. Phys. Soc. Jpn.*, 2003, **72**, 2369–2371.
31 S. Horiuchi, Y. Tokunaga, G. Giovannetti, S. Picozzi, H. Itoh, R. Shimano, R. Kumai and Y. Tokura, *Nature*, 2010, **463**, 789.